Accepted Manuscript online: 2025-11-17 Article published online: 2025-12-09



Original Article

# Leveraging $H_2$ Reduction, Hydrometallurgy, and Chlor–Alkali Electrolysis for Recycling Waste $LiCoO_2$ Electrode of Spent Li-ion Batteries

Jiayin Zhou‡, Jingdian Liu‡, Shaoyu Yang, Chao Xu, Xiaofei Guan

Affiliation addresses are listed at the end of the article.

## GRAPHICAL ABSTRACT

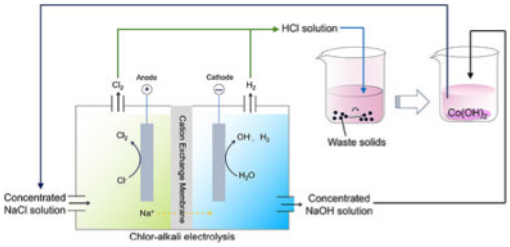


## ABSTRACT

The recycling of Li-ion batteries not only reduces the dependency on primary mineral resources but also mitigates environmental contamination associated with improper disposal. To advance the development of Li-ion battery recycling technologies, this study presents an integrative process for the recovery of waste $LiCoO_2$ by harnessing the advantages of $H_2$ reduction, hydrometallurgy, and chlor–alkali electrolysis. The waste $LiCoO_2$ was first treated with $H_2$ reduction roasting at 400 °C. The roasted product was then subjected to water leaching, achieving an Li leaching efficiency of ~96% within merely 5 min under 26 °C and a solid-to-liquid ratio of 1/14 g/mL, and resulting in a solid mixture of LiOH and $Li_2CO_3$ after evaporation and drying of the supernatant. Subsequently, the solid residue insoluble in the previous step of water leaching was subjected to HCl leaching and then NaOH precipitation to recover Co in the form of $Co(OH)_2$. Both the HCl and NaOH utilized can be derived from chlor–alkali electrolysis. Finally, the $Co(OH)_2$ and the mixture of LiOH and $Li_2CO_3$ recovered were used as raw materials to synthesize new $LiCoO_2$. Overall, this integrative process enables a closed loop, increases the utilization efficiency of HCl to near unity, and can in principle avoid the production of liquid or solid wastes.

**Keywords** Lithium-ion battery, $H_2$ reduction roasting, Leaching, Chlor–alkali electrolysis, Decoupling, Closed loop

**received** August 27, 2025 | **accepted after revision** November 10, 2025 | **article published online** 2025

**Bibliography** Sustainability & Circularity NOW **DOI** 10.1055/a-2749-6438 **Art ID** SCNOW-00059


‡ These authors contributed equally to this work.

**Correspondence** Prof. Xiaofei Guan, School of Physical Science and Technology, ShanghaiTech University, Huaxia Middle Road 393, 201210 Shanghai, China, Email: guanxf@shanghaitech.edu.cn
Prof. Chao Xu, School of Physical Science and Technology, ShanghaiTech University, Huaxia Middle Road 393, 201210 Shanghai, China, Email: xuchao1@shanghaitech.edu.cn

**Significance**

Unlike many works that center on advancing certain functional materials or optimizing a single isolated technology, this work harnesses the advantages of mature or viable technologies including $H_2$ reduction roasting, hydrometallurgy, and chlor-alkali process in combined yet decoupled manner. This integration is not merely a technical assemblage but a strategic design to construct a closed-loop system and achieve high performance for recycling the positive electrode materials of spent Li-ion batteries. This work contributes to the UN Sustainable Development Goals (e.g., 11, 12, 13).

## 1 Introduction

The spent Li-ion batteries have been dubbed as artificial minerals for the extraction of lithium and transition metals.[1] So far, various recycling technologies have been studied, including pyrometallurgy,[2] hydrometallurgy,[3] direct recycling,[4] and electrochemical methods.[5,6] In the recycling industry, pyrometallurgical and hydrometallurgical methods are often combined. The conventional pyrometallurgical processes have the advantages of scalability and compatibility with diverse Li-ion battery chemistries.[7,8] However, they typically require extremely high temperatures and large energy consumption, release harmful gases (e.g., HF, $CO_2$) during the smelting step, and have relatively low recovery efficiency of lithium.[9] In comparison, the hydrometallurgical processes typically use strong inorganic acid solutions to leach valuable metals.[10,11] The HCl solution in particular shows an excellent leaching performance, primarily attributed to the ability of chloride ions to destabilize the formation of a surface layer.[12] If $H_2SO_4$ is used as the leaching agent, reducing agents (e.g., $H_2O_2$, ethanol) are usually added to reduce the high-valence transition metal ions and enhance the leaching.[13,14]

The use of inorganic acids in hydrometallurgical processes is generally associated with limitations such as the generation of hazardous gases and liquids as well as the low acid utilization efficiency. In contrast, organic acids such as citric acid ($C_6H_8O_7$) and malic acid ($C_4H_6O_5$) have been explored due to their biodegradability and recyclability.[15] Nevertheless, their applications are limited by high costs, slow leaching kinetics, and low treatment capacity.[16] In recent years, electrochemical methods (e.g., electrolytic deposition,[17] slurry electrolysis,[18] electrolysis of aqueous solutions,[19,20] and molten salt electrolysis[21]) have demonstrated great potential in reducing the dependency on external sources of chemical reagents (e.g., acids, bases, and reducing agents), thereby lowering the consumption of chemicals and significantly decreasing the potential environmental hazards.

$H_2$ reduction has been demonstrated as a green and effective method as it not only transforms the lithium element into water-soluble chemicals but also reduces the valence states of transition metals in the waste positive electrode materials at around 500 °C, a much milder temperature than that of conventional pyrometallurgical methods (typically above 1000 °C).[20,22] Nonetheless, as reported in a recent work,[20] when the roasted products were leached in the anode chamber of a neutral water electrolyser, the acidic solution generated at the anode chamber reached only a moderate pH of 1.4–2.3, resulting in a relatively slow leaching kinetics of the transition metals.[20] To enhance the leaching kinetics, HCl solution can be added to the anode chamber of an NaCl aqueous solution electrolyser without an ion exchange membrane.[23] Nevertheless, the acid was consumed through chemical reactions with not only the waste positive electrode materials in the anode chamber but also the $OH^-$ diffused from the cathode chamber, severely limiting the acid utilization efficiency.[20,24] Given these issues, it is imperative to develop new strategies for further enhancing the leaching of transition metal ions and improving the acid utilization efficiency.

Unlike many existing works that center on optimizing a single isolated technology or advancing certain functional materials, this research adopts a holistic and integrative approach by synergistically combining $H_2$ reduction roasting, hydrometallurgical leaching and precipitation, and the industrially established chlor–alkali process for recycling the positive electrode materials of spent Li-ion batteries (**Fig. 1**). Specifically, the concentrated NaCl aqueous solution was electrolyzed (Eq. (1)) to form $Cl_2$ as the major gas product at the anode (Eq. (2)) along with $H_2$ and NaOH at the cathode (Eq. (3)).[25] The $H_2$ and $Cl_2$ can react to prepare a strongly acidic HCl solution (Eq. (3)).[26] Prior to the leaching with the HCl solution, the waste $LiCoO_2$ was first subjected to $H_2$ reduction roasting not only to transform the lithium element into the more soluble LiOH but also to reduce the trivalent cobalt in $LiCoO_2$ mainly to the divalent cobalt in CoO (Eq. (5)), with a minor amount of metallic cobalt also formed (Eq. (6)). The roasted product was then washed with de-ionized water, and the supernatant was concentrated to dryness, yielding solid powders containing mainly LiOH. The solid residue insoluble during the water leaching step was then processed in the concentrated HCl solution to leach out the $Co^{2+}$ (Eq. (7)) until the solution pH exceeded 5 (**Fig. 1b**). Afterward, the $Co^{2+}$ ions were precipitated in the form of $Co(OH)_2$ using the concentrated NaOH solution (Eq. (8)) obtained from the chlor–alkali electrolysis (**Fig. 1c**). The $Co(OH)_2$ and the lithium-containing compounds recovered were used as raw materials to resynthesize $LiCoO_2$ with enhanced electrochemical performance.

Compared with the previous work,[20] this work represents a significance advancement. Specifically, this work is focused on a new and practical integrative process comprising $H_2$ reduction roasting, hydrometallurgical leaching and precipitation, and chlor–alkali electrolysis in a combined yet decoupled manner. The reliance on NaCl solution electrolysis for providing HCl and NaOH here is a key mechanistic difference that directly addresses the low leaching efficiency, low acid utilization efficiency, and high temperature limitations of the neutral-water electrolysis system with aqueous $Na_2SO_4$ electrolyte reported previously,[20] leading to significantly enhanced performance. This shift is also critically important for future industrial applications, as the chlor–alkali electrolysis using membrane cell technology is a mature industrial process with a high technological readiness level and high cost-effectiveness. This work also has a different methodological design. For example, the $H_2$ roasted product is subjected to the water leaching and the HCl acid leaching in sequence, causing Li and Co to be leached out successively and making their separation easier. In addition, the Li element is recycled mainly in the form of LiOH with $Li_2CO_3$ as the secondary phase. The objective of this study

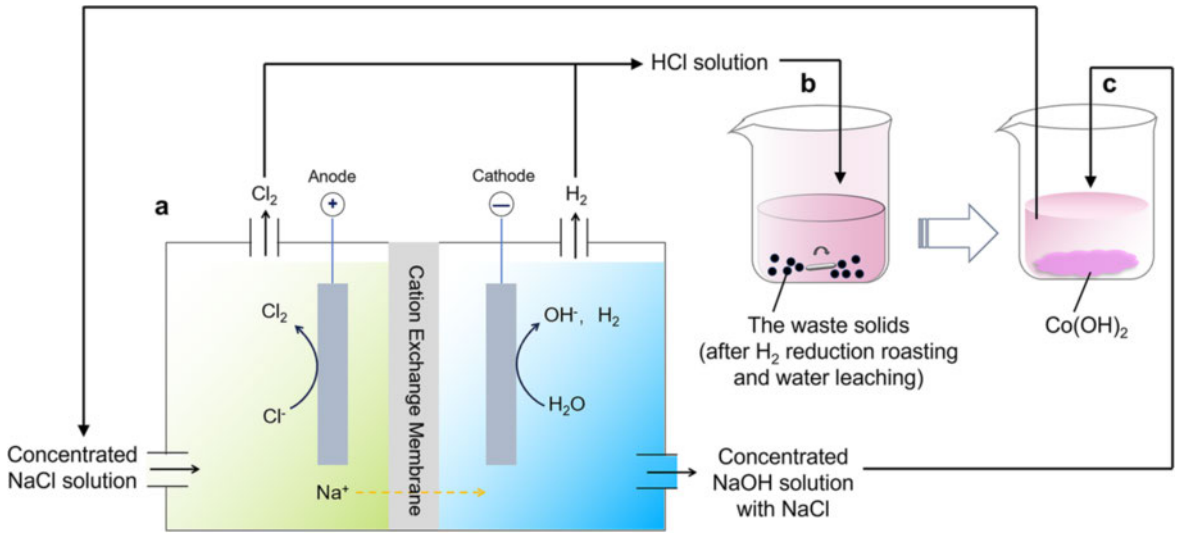


**Fig. 1** Conceptual illustration of an integrated process for recycling waste positive electrode material (e.g., $LiCoO_2$) of spent Li-ion batteries. (**a**) Chlor–alkali electrolyser equipped with a cation exchange membrane to produce $H_2$ and NaOH at the anode and $Cl_2$ at the anode. $H_2$ and $Cl_2$ can react to produce HCl. (**b**) HCl solution leaching of the solid waste material that was obtained after $H_2$ reduction roasting of pristine waste $LiCoO_2$ and water leaching. (**c**) Precipitation of the $Co^{2+}$ in the form of $Co(OH)_2$ using the concentrated NaOH solution derived from the chlor–alkali electrolysis. After separating the $Co(OH)_2$ precipitates, the supernatant can be neutralized and reused as the electrolyte in the chlor–alkali electrolysis.

is to provide a proof-of-concept demonstration of this integrative approach for the effective recycling of the waste $LiCoO_2$ materials. The innovation of this work is the system-level combination of mature or viable technologies to enable a closed loop, reduce the generation of hazardous wastes, and achieve effective recycling of waste positive electrodes of spent Li-ion batteries. Overall, this method aligns with the core tenets of circular chemistry and sustainability.[27–29] It has great potential for delivering a robust solution for recycling the positive electrode materials of spent Li-ion batteries and enhancing the research's adaptability and scalability.

$$2NaCl + 2H_2O \rightarrow 2NaOH + H_2(g) + Cl_2(g) \quad (1)$$

$$2Cl^- - 2e^- \rightarrow Cl_2(g) \quad (2)$$

$$2H_2O + 2e^- \rightarrow 2OH^- + H_2(g) \quad (3)$$

$$H_2(g) + Cl_2(g) \rightarrow 2HCl \quad (4)$$

$$LiCoO_2 + 1/2H_2(g) \rightarrow CoO + LiOH \quad (5)$$

$$CoO + H_2(g) \rightarrow Co + H_2O(g) \quad (6)$$

$$CoO + 2HCl(a) \rightarrow Co^{2+} + 2Cl^- + H_2O \quad (7)$$

$$Co^{2+} + 2OH^- \rightarrow Co(OH)_2 \quad (8)$$

## 2 Results and Discussion

### 2.1 $H_2$ reduction roasting of $LiCoO_2$ and the subsequent water leaching

To enhance the leaching kinetics of $LiCoO_2$ in acids, 5%$H_2$–95%Ar was first utilized as a reductant to calcine the waste $LiCoO_2$ at 400°C for 200 min. Based on the XRD characterization of the roasted product (**Fig. 2a**), the pristine $LiCoO_2$ phase disappeared; instead, CoO as the major phase along with Co and LiOH as the minor phases were identified. Among them, LiOH was readily soluble in water, whereas CoO and Co were insoluble. Therefore, water leaching was employed to selectively dissolve LiOH and separate lithium from cobalt.

To investigate the factors influencing the leaching efficiencies of Li and Co in water, a series of experiments were conducted with varying temperatures, durations, and solid-to-liquid ratios. Subsequently, the preferred conditions for water leaching of the roasted products were determined. **Fig. 2b** shows the effect of temperature (26, 43, 60, 72, and 85 °C) on the leaching efficiencies of Li after the experiments with the same duration (45 min) and solid-to-liquid ratio (1/7 g/mL; prepared by adding 1 g sample to 7 mL de-ionized water). The Li leaching efficiency reached a high value of ~87% at 26 °C and increased further to ~94% as the temperature increased to 85 °C. Given the relatively limited increase in the Li leaching efficiency, the preferred temperature was selected as 26 °C for energy savings. Note that the Co leaching efficiency in water was below the detection limit of ICP-OES at all the tested temperatures, indicating the effectiveness of water leaching for separating Li from Co.

**Fig. 2c** illustrates the leaching efficiencies of Li under various durations (5, 10, 25, 45, and 65 min) in the experiment with the solid-to-liquid ratio of 1/7 g/mL at 26 °C. The leaching efficiency of Li reached ~86% after only 5 min of leaching. When the leaching duration increased to 65 min, the leaching efficiency of Li only improved slightly. Therefore, the preferred duration for water leaching was chosen as 5 min to save time. Similar to the results in the aforementioned experiments, the Co leaching efficiency in water remained below the detection limit.

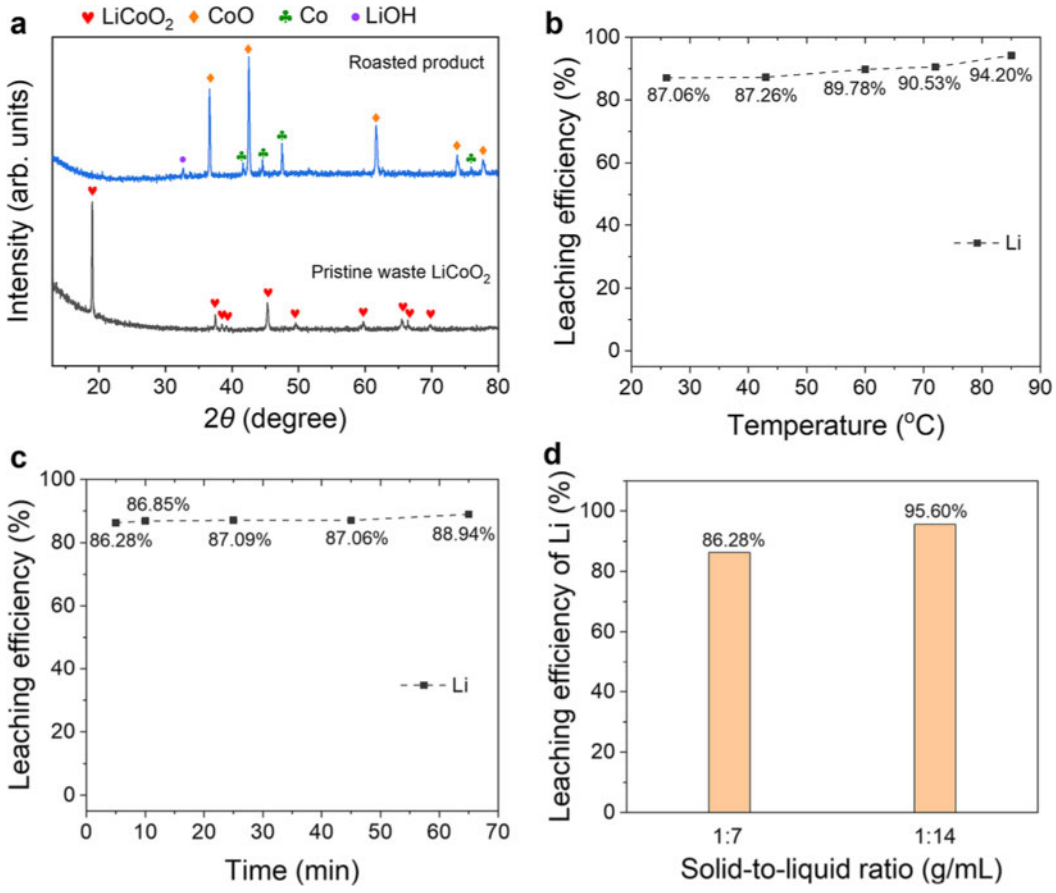


**Fig. 2** (**a**) The XRD patterns of the pristine waste $LiCoO_2$ and the roasted product after $H_2$ reduction roasting at 400 °C for 200 min in 5%$H_2$–95%Ar. The data from the standard powder diffraction file (PDF) cards for $LiCoO_2$ (PDF No. 01-075-3201), CoO (PDF No. 01-076-3830), Co (PDF No. 00-005-0727), and LiOH (PDF No. 00-004-0708) were used to index the diffraction peaks. The leaching efficiencies of Li and Co during water leaching under various conditions: (**b**) different temperatures (26, 43, 60, 72, and 85 °C), leaching duration of 45 min, and solid-to-liquid ratio of 1/7 g/mL; (**c**) temperature of 26 °C, different durations (5, 10, 25, 45, and 65 min), and solid-to-liquid ratio of 1/7 g/mL; (**d**) temperature of 26 °C, leaching duration of 5 min, and different solid-to-liquid ratios (1/7 and 1/14 g/mL). Leaching efficiency data in panels b–d retain two decimal places for clearer trend visualization; actual precision aligns with error analysis (2 significant digits).

To investigate the effect of the solid-to-liquid ratio on the Li leaching efficiency in water, two experiments were conducted for 5 min at 26 °C with different solid-to-liquid ratios of 1/7 and 1/14 g/mL, respectively. In these experiments, 0.5 or 1 g of roasted products were added to 7.0 mL de-ionized water, respectively. **Fig. 2d** depicts that decreasing the solid-to-liquid ratio from 1/7 to 1/14 g/mL enhanced the Li leaching efficiency from ~86% to ~96%. A relatively higher ratio of water facilitated an increased leaching of Li. Consequently, the preferred solid-to-liquid ratio for Li leaching was chosen as 1/14 g/mL. To further demonstrate the reproducibility, additional water leaching experiments were performed under 22 °C for 5 min with different solid-to-liquid ratios (1/7 and 1/14 g/mL). **Fig. S1** depicts the leaching efficiency of Li under these two conditions with error bars derived from two replicates per condition, showing the consistent trend as that in **Fig. 2d**.

After water leaching of the roasted products under the selected conditions (temperature of 26 °C, leaching duration of 5 min, and solid-to-liquid ratio of 1/14 g/mL), the clear supernatant was separated from the solid residue using centrifugation followed by an extra step of vacuum filtration. The supernatant was subjected to heat treatment at ~100 °C for evaporation until dryness, and the solid white powders acquired were identified as mainly consisting of LiOH based on XRD analysis, with $Li_2CO_3$ as the secondary phase (**Fig. S2**). The formation of $Li_2CO_3$ was likely attributed to the following two factors: Firstly, a small amount of carbon was present in the waste positive electrode materials; it reacted with the waste $LiCoO_2$ positive electrode material, generating trace amounts of $Li_2CO_3$ during the $H_2$ reduction roasting step (Eq. (9)).[31] Secondly, anhydrous LiOH spontaneously reacted with $CO_2$ in the air during the drying and the sample transfer (Eq. (10)).[32] In addition to XRD, the XPS was also used to characterize the solid white powders. In the XPS survey spectrum, all the major peaks were attributed to the O, C, and Li, suggesting the arrbsence of impurities (**Fig. S3a**). The core-level C 1*s* XPS spectrum revealed the presence of two distinct types of carbon on the sample surface (**Fig. S3b**). The peak close to 284.8 eV was attributed to adventitious carbon, while another major peak near 289.8 eV was assigned to the carbonate.[33,34] The undissolved residue obtained from the water leaching

experiment was also characterized to be CoO as the major phase and Co as the minor phase with XRD (**Fig. S4**). The undissolved residue in water was treated in the subsequent HCl solution leaching experiments to mainly extract the $Co^{2+}$ ions (**Fig. 1b**).

$$4LiCoO_2 + C \rightarrow 4CoO + Li_2O + Li_2CO_3 \quad (9)$$

$$2LiOH + CO_2(g) \rightarrow Li_2CO_3 + H_2O \quad (10)$$

## 2.2 Electrolysis of NaCl Solution

A 5 mol/L NaCl solution was subjected to a constant-current electrolysis at 0.8 A for 6 h at 77 °C in an H-cell (**Fig. 1a**). Electrochemical impedance spectroscopy (EIS) was performed between the anode and cathode before electrolysis, and the cell ohmic resistance was measured to be 6.9 Ω (**Fig. S5a**). The applied voltage vs. time curve recorded during the electrolysis process is depicted in **Fig. S5b**, indicating only slight fluctuations in voltage throughout the electrolysis. After the electrolysis, the catholyte became strongly alkaline, with the pH value measured to be 13.8 ($[OH^-]$ = 0.631 mol/L). The catholyte was collected to act as the precipitating agent for $Co^{2+}$ in the subsequent precipitation experiments. The analyte pH was measured to be around 5. After adding more NaCl and proper neutralization, the anolyte can be in principle reused as electrolyte in further cycles of electrolysis experiments.

The cation exchange membrane in the H-cell performed dual critical functions: firstly, as a physical barrier, it prevented the transport of oxidative species (e.g., $Cl_2$, $ClO^-$, and $ClO_3^-$)[35] generated in the anode chamber toward the cathode chamber; secondly, it contributed to the elevation of the catholyte alkalinity after the 6-h electrolysis. In comparison, in a control experiment without using a cation exchange membrane, the alkalinity of the catholyte after a 6-h constant-current electrolysis at 0.8 A at 77 °C was measured to be significantly lower (pH = 12.4 and $[OH^-]$ = 0.025 mol/L).

During the electrolysis of a 5 mol/L NaCl solution, the primary anodic reaction was the chlorine evolution reaction (CER; Eq. (2)). Note that the oxygen evolution reaction (OER; $2H_2O - 4e^- \rightarrow O_2(g) + 4H^+$) also occurred simultaneously as a competing side reaction. Thermodynamically, the OER was more favorable than the CER under standard conditions. Nevertheless, the use of commercial Dimensionally Stable Anode (DSA) electrodes can effectively lower the activation energy barrier of CER, improving the $Cl_2$ selectivity.[35] To estimate the molar ratio of $Cl_2$ to $O_2$ generated in the anode chamber, another experiment was performed, in which the H-cell containing 5 mol/L NaCl solution was heated to 77 °C, and pure $N_2$ carrier gas was introduced at 8.1 mL/min to first purge the air out of the anode chamber. The effluent gas out of the anode chamber was passed to two absorption chambers containing 5 mol/L NaOH solution (200 mL in one and 500 mL in the other) in sequence for absorbing any $Cl_2$ generated during the subsequent electrolysis. The effluent gas was then passed to a drying column containing $CaCl_2$ pellets before directing to a gas chromatograph (GC) to monitor the effluent gas composition. After ensuring that the air was completely removed, a constant-current electrolysis at 0.8 A was initiated. Based on the GC measurements, the $O_2$ generation rate gradually increased with electrolysis time and reached a relatively steady value of 0.25 mL/min after 600 min (**Fig. S6**). Based on the $O_2$ generation rate and the electrolysis current, the proportion of $O_2$ in the gas produced at the anode was estimated to be 2–3%, verifying the high $Cl_2$ selectivity (97–98%). The anodic product of $Cl_2$ and the cathodic product of $H_2$ can react for preparing the HCl solution.[26] Due to the stringent reaction conditions required, the reaction for synthesizing HCl was not conducted in the laboratory. Nonetheless, this reaction is highly feasible and well established in industrials settings. Therefore, only a descriptive account of this reaction is provided here. We opted to utilize commercially available concentrated HCl solution as an alternative. The HCl solutions of the desired concentrations (0.1, 1, and 2 mol/L) were prepared and utilized to leach the solid powders acquired after conducting the $H_2$ reduction roasting of the waste $LiCoO_2$ and the water washing.

## 2.3 HCl Leaching and NaOH Precipitation

### 2.3.1 HCl Leaching

The solid powders undissolved in the water leaching step were separated and then leached in the HCl solution (**Fig. 1b**). **Table 1** shows the experimental details on total masses of solid powders added, volumes and initial concentrations of HCl solutions, and pH values after leaching in different experiments. Adding the solid powders to the acid leaching solution at once could slow the

**Table 1** Experimental details on the HCl solution leaching experiments using the setup as shown in **Fig. 1b**. The solid powders were acquired after conducting the $H_2$ reduction roasting of waste $LiCoO_2$ and the water leaching. Each acid leaching experiment had two equal-duration stages, with one batch of samples processed per stage.

| Experiment label | Total mass of solid powders added (g) | Volume of HCl solution (mL) | Total leaching time (h) | Initial concentration of HCl solution (mol/L) | pH of solution after HCl leaching | HCl utilization efficiency calculated |
|---|---|---|---|---|---|---|
| I-a | 0.245 | 6 | 1 | 0.1 | 6.45 | Near unity |
| I-b | 0.245 | 6 | 0.5 | 0.1 | 6.48 | |
| I-c | 0.245 | 6 | 0.5 | 0.1 | 6.29 | |
| II | 0.528 | 6 | 6 | 1 | 6.15 | |
| III | 0.606 | 6 | 4 | 2 | 5.88 | |
| IV | 1.508 | 10 | 4 | 2 | 5.56 | |
| V | 3.936 | 40 | 6 | 2 | 6.38 | |

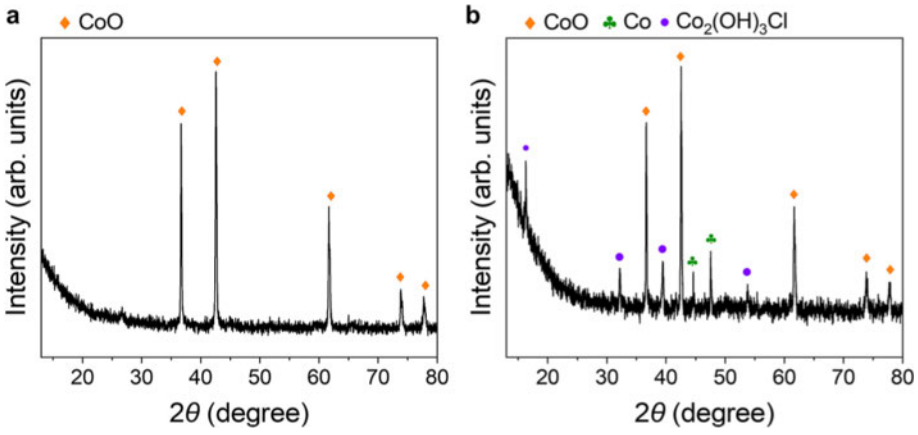


**Fig. 3** XRD patterns of (**a**) the residues after leaching the first batch of solid powders for 2 h and (**b**) the residues after leaching the second batch of solid powders for 2 h in experiment IV. The data from the PDF cards for CoO (PDF No. 01-076-3830), Co (PDF No. 00-005-0727), and $Co_2(OH)_3Cl$ (PDF No. 01-075-7688) were used to index the diffraction peaks. The starting leachate was 10 mL 2 mol/L HCl solution. The solid powders used were acquired after conducting the $H_2$ reduction roasting of waste $LiCoO_2$ and the water leaching.

dissolution. To ensure more complete dissolution and maximize the utilization of acid in the solution, the solid powders were added in two separate batches in those experiments.

The experiments labeled as I-b and I-c were replicated experiments using the same total mass of solid powders (~0.245 g) with the same total leaching time (0.5 h). In these experiments, the first batch of solid powders (~0.122 g) were added to 6 mL of 0.1 mol/L HCl solution. After 15 min of acid leaching, the remaining solid powders were filtered out; and the second batch of solid powders (~0.123 g) was added to fully take advantage of the remaining acid in the leaching solution. After another 15 min of acid leaching, the pH values of the leaching solutions in these duplicated experiments increased to ~6.48 and ~6.29, respectively. The close values validated the reproducibility of these experiments. Note that Experiment I-a just had a slightly longer total leaching time (1 h), and the final pH value (~6.45) was also similar.

Experiment IV used a relatively large amount of solid powders, making the postreaction materials easier to collect and characterize, and so the detailed characterization results and the relevant discussions for Experiment IV are elaborated as a representative. In Experiment IV, the first batch of solid powders (~0.846 g) were added to 10 mL 2 mol/L HCl solution. After 2 h of the acid leaching, the solution turned pink, indicating the effective leaching of $Co^{2+}$ from the solid powders into the solution. The pH value of the leaching solution increased but still slightly less than 0. The remaining solid powders were filtered out, washed with 10 mL de-ionized water for three times, dried in oven, and then characterized to be CoO with XRD (**Fig. 3a**). To further take advantage of the remaining acid in the leaching solution, the second batch of solid powders (~0.662 g) acquired from the water leaching step was added. After another 2 h of acid leaching, the pH value of the leaching solution rose significantly to ~5.56. Based on the initial and final acidity of the HCl leaching solution, the acid utilization was calculated to be near unity using Eq. (12). The remaining solid powders were again filtered out, washed three times with de-ionized water, dried, and then characterized to be a mixture of CoO, Co, and $Co_2(OH_3)Cl$ with XRD (**Fig. 3b**). The $Co_2(OH)_3Cl$ phase was considered as a solid solution of $Co(OH)_2$ and $CoCl_2$,[36] and its formation was likely promoted by the sufficient $Cl^-$ in the weakly acidic solution. As both CoO and $Co_2(OH)_3Cl$ could dissolve in the HCl solution of strong acidity to release the $Co^{2+}$ ions,[36] all the remaining solid powders can be leached again by adding them to new strongly acidic HCl solution in another round of acid leaching experiment. Therefore, the generation of solid cobalt-containing waste would in principle be negligible by following those procedures. It is also noted that all the experiments in **Table 1** pointed to the same conclusion on the near-unity HCl utilization efficiency. Such cross-experiment consistency provides support for the robustness of the findings.

It is worthing mentioning that the signals of Co metal were detected in the residues after the leaching of the second batch of solid powders (**Fig. 3b**) but not after the leaching of the first batch (**Fig. 3a**) in Experiment IV. The results were reasonable because they were attributed to the significant difference in the pH environment between the two leaching stages. Specifically, during the leaching of the first batch of solid powders in Experiment IV, the leaching solution still retained a very low pH (less than zero), thereby efficiently leaching the Co element (**Fig. 3a**). In contrast, at the end of the stage of leaching the second batch of solid powders, the pH of the leaching solution had risen significantly to ~5.56 due to the consumption of acid. This near-neutral pH environment resulted in a much weaker acidity, insufficient to dissolve the additional Co element, thus leaving some metallic Co detectable in the residues from the second batch (**Fig. 3b**).

### 2.3.2 NaOH Precipitation

A portion of the weakly acidic solution obtained from the HCl leaching experiment was added to the alkaline solution (pH = 13.8) obtained from NaCl solution electrolysis. Blue α-$Co(OH)_2$ precipitates were initially formed, which gradually turned into pink β-$Co(OH)_2$.[37] The precipitates were then separated using

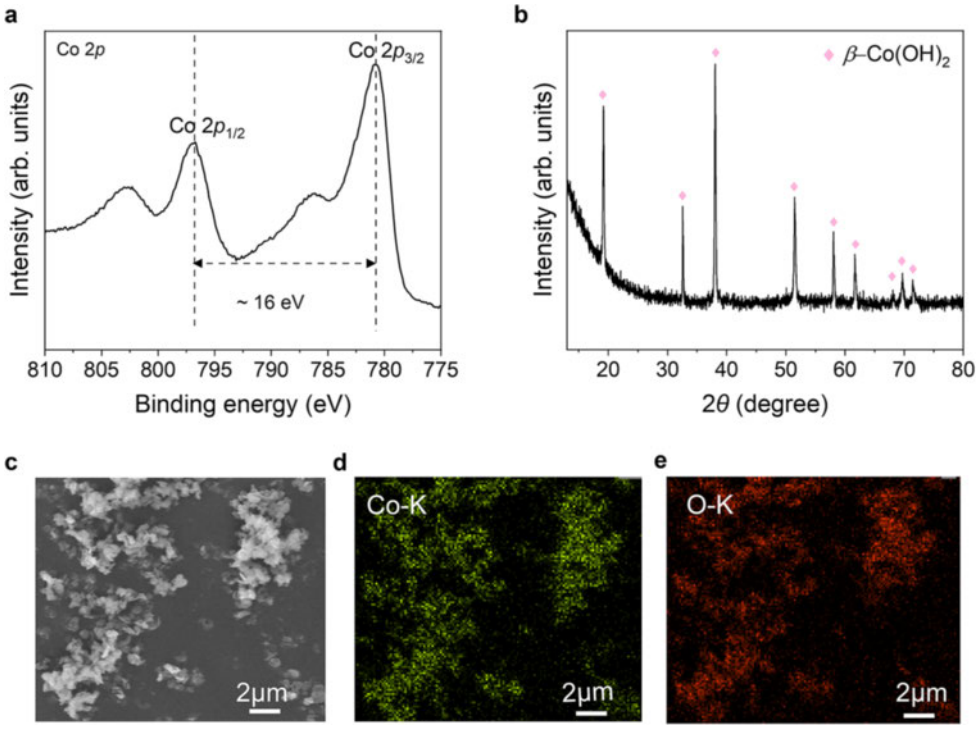


**Fig. 4** (**a**) High-resolution Co 2p XPS result, (**b**) XRD pattern, (**c**) SEM image of the precipitates and the corresponding EDS mapping of the elements of (**d**) Co and (**e**) O. In panel b, the data from the PDF card for $Co(OH)_2$ (PDF No. 00-030-0443) were used to index the diffraction peaks.

centrifugation, dried, and then characterized. The XPS survey scan of the precipitates exhibited mainly the signals of the Co, O, and C elements (**Fig. S7**). The high-resolution Co 2p XPS result showed the spin-orbit peaks of Co $2p_{3/2}$ and Co $2p_{1/2}$ at ~780.8 and ~796.8 eV, respectively; the difference between the two peaks was ~16 eV (**Fig. 4a**), confirming that the cobalt primarily existed in the +2 oxidation state. In the XPS survey scan (**Fig. S7**), the signal centering at ~285 eV represented the adventitious carbon, which might originate from hydrocarbon pollutions adsorbed on the sample surface when it was exposed to the ambient atmosphere or the handling environment.

The XRD pattern of the precipitates displayed characteristic peaks of β-$Co(OH)_2$ (**Fig. 4b**). The SEM images of the precipitates showed sheet-like morphology (**Fig. 4c**; see Figure S8 for greater magnification). The EDS mapping on the area shown in **Fig. 4c** confirmed the homogeneous distribution of the Co and O elements throughout the precipitates (**Fig. 4d, e**). Note that after separating the $Co(OH)_2$ precipitates, the supernatant may be neutralized and reused as the electrolyte in the NaCl solution electrolysis, closing the material loop (**Fig. 1**).

## 2.4 Synthesis of $LiCoO_2$ and Its Electrochemical Performance

Compared to using $Li_2CO_3$ alone as the lithium precursor, the decomposition temperature of $Co(OH)_2$ can be effectively reduced when $LiOH{\cdot}H_2O$ or a mixture of $LiOH{\cdot}H_2O$ and $Li_2CO_3$ is employed as the lithium source.[38] In this work, the $Co(OH)_2$ precipitates and the mixture of LiOH and $Li_2CO_3$ recovered were used as raw materials to synthesize new $LiCoO_2$. The materials were mixed according to a 1:1 Li:Co molar ratio, and the resulting product was referred to as LCO_100. The XRD pattern showed that the main phase was $LiCoO_2$ with a space group of $R\bar{3}m$ (**Fig. 5a**). As both the $Co(OH)_2$ precipitates and the $LiOH–Li_2CO_3$ mixture were obtained without any morphology control, it was necessary to evaluate and compare the electrochemical performance of the $LiCoO_2$ synthesized with that of the $LiCoO_2$ prepared from commercial chemical reagents. Therefore, $LiCoO_2$ powders, referred to as LCO_$LiOH/Li_2CO_3$, were synthesized using commercial $Co(OH)_2$, $LiOH{\cdot}H_2O$, and $Li_2CO_3$ with an Li:Co molar ratio of 103% under the same sintering conditions. The corresponding XRD pattern is presented in **Fig. 5b**. The powder prepared from commercial reagents mainly consisted of the $LiCoO_2$ phase. The SEM images of LCO_100 and LCO_$LiOH/Li_2CO_3$ are shown as insets in **Fig. 5a, b**, respectively. Both samples exhibited similar particle sizes and irregular morphologies.

The electrochemical cycling performances of both LCO_100 and LCO_$LiOH/Li_2CO_3$ were evaluated using coin cells, and the results are shown in **Fig. 5c, d**. At a low current density of 20 mA/g (0.1C), both materials exhibited comparable charge and discharge capacity (**Fig. 5c**). Upon increasing the rate to 1C (200 mA/g), LCO_100 exhibited a capacity retention of approximately 97.3% after 100 cycles, whereas LCO_$LiOH/Li_2CO_3$ showed a much lower capacity retention of around 60.5% (**Fig. 5d**). Based on the above results, the $LiCoO_2$ synthesized from the recovered materials demonstrated better electrochemical performance than the $LiCoO_2$ prepared from commercial cobalt and lithium

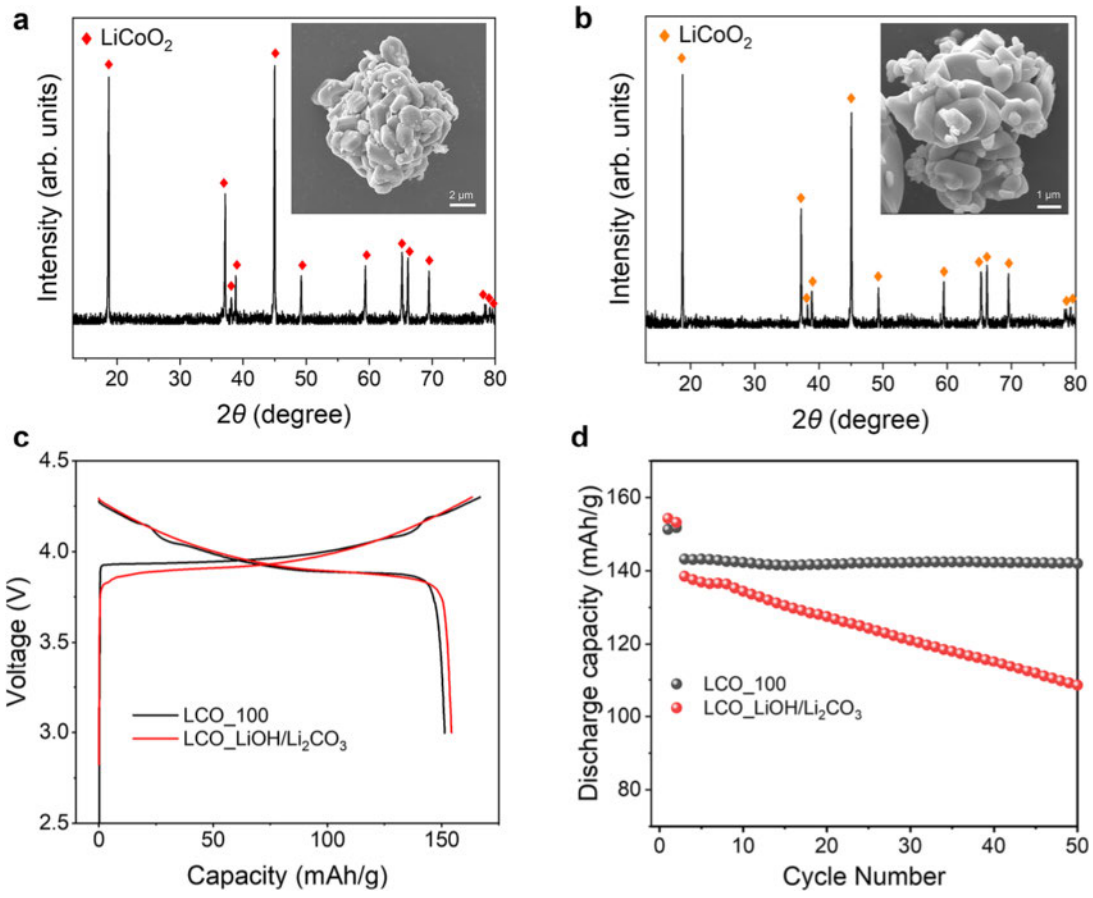


**Fig. 5** XRD patterns of (**a**) the LCO_100 prepared from the materials recovered and (**b**) the LCO_LiOH/$Li_2CO_3$ prepared from commercial reagents. (**c**) The charge/discharge curves and (**d**) cycling performance of the coil cells with LCO_100 or LCO_LiOH/$Li_2CO_3$ as the positive electrode.

salts, showing great promise for this recycling technology. Nevertheless, it is worth noting that a single test may not fully support the conclusion that the recovered materials provide better electrodes. Comprehensive supplementary tests, including long-cycle stability and multibatch reproducibility experiments, are necessary to fully validate the performance of the electrodes prepared from the recovered materials.

Considering the wide variety of positive electrode materials currently used in commercial lithium-ion batteries, it is highly desirable for a recycling process to be capable of handling mixed positive electrode materials. The proposed method demonstrates the potential of broad applicability beyond $LiCoO_2$. It can also be employed for the recovery of other valuable cathode materials such as $LiMn_2O_4$ and $LiNi_xMn_yCo_zO_2$ (NMC). After $H_2$ reduction roasting, $LiMn_2O_4$ can be transformed into MnO and $Li_2O$.[39] $Li_2O$ can be efficiently dissolved with water, and the MnO can be subsequently leached using acidic solutions to recover $Mn^{2+}$. Similarly, $LiNi_xMn_yCo_zO_2$ can be transformed into metallic or metal oxide phases containing Ni, Co, and Mn after $H_2$ reduction roasting.[40] Following acid leaching, a solution rich in mixed transition metal ions is obtained, which can then be processed via coprecipitation methods to synthesize NMC precursors.[41]

## 3 Conclusions

In summary, this work has presented a sustainable and circular process comprising $H_2$ reduction roasting, hydrometallurgy, and chlor–alkali electrolysis in a combined yet decoupled manner for the recycling of waste positive electrode materials of Li-ion batteries. The leaching efficiency of Li reached 96% within 5 min when the roasted products were leached in de-ionized water under 26 °C and a solid-to-liquid ratio of 1/14 g/mL. Following evaporation and concentration of the Li-containing supernatant, lithium was recovered in the form of a mixture of LiOH and $Li_2CO_3$. The solid residue insoluble during water leaching was separated and then leached in HCl solution, and the utilization efficiency of the acid reached near unity. The $Co^{2+}$ ions were precipitated in the form of $Co(OH)_2$ using the NaOH solution produced by the chlor–alkali electrolysis. The $Co(OH)_2$ precipitates were calcined with the lithium-containing mixture recovered, successfully synthesizing $LiCoO_2$ with high electrochemical performance (e.g., retaining 97.3% capacity after 100 charge-discharge cycles), outperforming batteries that used its counterpart synthesized from commercial reagents. Comprehensive supplementary battery tests are still needed to validate this aspect. Overall, the integrated approach represents a promising pathway for the green

and sustainable recycling of the waste positive electrode materials of spent Li-ion batteries.

# 4 Experimental Section

## 4.1 Disassembly and Pretreatment

Spent $LiCoO_2$ batteries were obtained from recycling merchants and then disassembled manually in a lab fume hood (**Fig. S9**). Subsequently, the positive electrode materials were separated following the pretreatment procedures as described in a previous work.[24] The positive electrode powders separated, referred to as pristine powders, were treated with $H_2$ reduction roasting in the following experiments.

## 4.2 $H_2$ Reduction Roasting

Pristine waste $LiCoO_2$ powders (~6 g) were added into an alumina boat and then transferred to a quartz tube sealed with vacuum flanges inside a horizontal electric furnace. The operation temperature was ramped to 400 °C at a rate of 5 °C/min while maintaining an inert Ar atmosphere. Once the temperature reached 400 °C, the Ar feeding gas was switched to 5%$H_2$–95%Ar gas at 180 $cm^3$/min. After 200 min of $H_2$ reduction roasting, the feeding gas was switched back to Ar, and the furnace was cooled to room temperature at a rate of 5 °C/min. The purity of the gases (Shanghai Wetry™ Standard Gas Analysis Technology Co., Ltd., Shanghai, China) used were greater than 99.999%.

## 4.3 Water Leaching of the Roasted Products

Proper amounts of the roasted products obtained after the $H_2$ reduction were leached with de-ionized water in glass beakers (inner diameter: 2.7 cm; height: 4.0 cm) under varying conditions of temperature, time, and solid-to-liquid ratio. The solid-to-liquid ratio (unit: g/mL) here was defined as the ratio of the mass of the roasted products to the volume of the de-ionized water. A magnetic stirring bar was used at 300 rpm to facilitate the leaching. After each water leaching experiment, the supernatant was separated from the undissolved solid powders using centrifugation (5000 rpm, 4 min × 2; Sunne™, Shanghai, China; Product No.: SN-LSC-3A). The supernatant was further treated with vacuum filtration using quantitative filter paper (Titan™, Shanghai, China; Part No.: 202; diameter: 9 cm).

The supernatant was sampled using a micropipette, diluted by adding 1 mol/L HCl solution, and then analyzed with ICP-OES to determine the concentration of the Li element. The total mass of Li element in the supernatant ($m_{Li,supernatant}$) was equal to the product of the concentration of Li element in the supernatant ($C_{Li,supernatant}$; unit: μg/mL) and the volume of the supernatant ($V_{Li,supernatant}$; unit: mL). To determine the total amount of Li element in the roasted products, 0.05 g of roasted products were dissolved in 10 mL concentrated HCl solution (36.5 vol%) for 20 h. After centrifugation, the solution was treated with vacuum filtration, diluted, and then analyzed with ICP-OES to determine the $Li^+$ concentration. The total mass of Li element in the roasted products ($m_{Li,roasted\ products}$) was calculated as the product of the concentration of Li element in the concentrated HCl solution ($C_{Li,roasted\ products}$; unit: μg/mL) and the volume of the concentrated HCl solution ($V_{Li,roasted\ products}$; unit: mL). The leaching efficiency of Li element during the water leaching of the roasted products ($\eta_{Li}$) was determined using Eq. (11) below. The input with the fewest significant figures was $V_{Li,supernatant}$ = 7.0 mL (2 significant figures), setting the precision bottleneck for $\eta_{Li}$ based on the relative error propagation rules.

$$\eta_{Li} = \frac{m_{Li,supernatant}}{m_{Li,roasted\ products}} = \frac{C_{Li,supernatant} \times V_{supernatant}}{C_{Li,roasted\ products} \times V_{roasted\ products}} \quad (11)$$

## 4.4 Two-chamber H-Cell for the Electrolysis of 5 mol/L NaCl

Electrolysis was carried out in the H-shaped electrochemical cell (H-cell), comprising two borosilicate glass chambers (250 mL each) connected by a cross tube.[30] Commercial dimensionally stable anode (DSA; $RuO_2/IrO_2$-coated Ti plate; size: 3 cm × 5 cm × 1 mm; Suzhou Shuertai™ Industrial Technology Co., LTD, China) and Pt-coated Ti plate (size: 5 cm × 3 cm × 1 mm; Yiwanlin™ Electronic Technology, Kunshan, China) were used as the anode and the cathode, respectively. They were placed separately in the anode and cathode chambers containing NaCl aqueous electrolyte (5 mol/L; volume in each chamber: 150 mL; Aladdin). A cation-exchange membrane (Hangzhou Huamo™ Co., China; Part No.: GSCEM360) was fixed in the middle of the cross tube of the H-cell. All electrochemical measurements were conducted using a Gamry™ Interface 1000 potentiostat.

## 4.5 HCl Leaching and NaOH Precipitation

HCl solutions of different concentrations and volumes were prepared in 50 mL glass beakers. Desired amounts of the solid residues insoluble in the water leaching were weighed and added to those beakers containing HCl solutions. With magnetic stirring at 300 rpm, the solid residues were leached until the pH exceeded 5. The HCl utilization efficiency ($\eta_{HCl}$) was given by Eq. (12), where $C_i$ and $C_f$ were the initial and final concentrations of HCl in the acid leaching solution, respectively. The volume change of the acid leaching solution was assumed to be negligible.

$$\eta_{HCl} = \frac{C_i - C_f}{C_i} \quad (12)$$

After the leaching, the solution containing $Co^{2+}$ was separated from the undissolved residues via a centrifuge. Those undissolved residues were collected and further dissolved in a different round of acid leaching experiment. Afterward, 200 μL of the $Co^{2+}$-containing leachate was pipetted to determine the $Co^{2+}$ concentration using inductively coupled plasma-optical emission spectrometry (ICP-OES), based on which the minimum amount of NaOH required to precipitate the $Co^{2+}$ was calculated.

## 4.6 Synthesis of $LiCoO_2$

The $Co(OH)_2$- and the Li-containing mixture recovered was analyzed to determine the exact amounts of Co and Li, respectively, based on which the materials were weighed and mixed to achieve an Li:Co molar ratio of 1:1. After thoroughly grinding with a mortar and pestle, the mixed powders were placed in an alumina crucible for calcination at 850 °C for 12 h under pure $O_2$ atmosphere.

The heating rate was set to 4°C/min. The resulting product was labeled as LCO_100.

For comparison, commercial $Co(OH)_2$, $LiOH{\cdot}H_2O$, and $Li_2CO_3$ were also used as raw materials to synthesize $LiCoO_2$. In the starting materials, the Li:Co molar ratio was 1.03:1, and the $LiOH{:}Li_2CO_3$ mass ratio was ~0.71:0.29. Specifically, 0.87 g of $Co(OH)_2$, 0.31 g of $LiOH{\cdot}H_2O$, and 0.072 g of $Li_2CO_3$ were thoroughly ground with a mortar and pestle and then calcined under the same conditions as above. The resulting product was labeled as $LCO\_LiOH/Li_2CO_3$.

Each calcined product (~0.21 g) was mixed with Super–P carbon black and vinylidene fluoride (PVDF) with a weight ratio of 8:1:1 in N–methyl pyrrolidine (NMP) using a THINKY™ mixer. The slurries were cast on Al foils and dried in a vacuum oven at 100 °C overnight. Circular electrodes with a diameter of 12 mm were punched out, and the typical loading of active materials was 4.5 $mg/cm^2$. The electrolyte consisted of 1.0 M $LiPF_6$ dissolved in ethylene carbonate (EC)–ethyl methyl carbonate (EMC) (3:7 by volume). Glass fiber (GF/D) was used as the separator. Coin cells (CR 2032-316) were assembled in an Ar–filled glovebox (Vigor™; $O_2$ and $H_2O$ levels less than 0.2 ppm) with Li foil as the counter electrode. Battery testing was performed using a Landt™ CT3002A battery tester in a temperature-controlled environment (25 °C).

## 4.7 Material Characterization

The crystalline structures of the samples were determined using X-ray diffraction (XRD, Bruker™ D8; copper target; θ–2θ geometry). The XRD patterns were scanned with an increment of 0.02 ° and a dwell time of 0.2 s per step, followed by phase identification based on either previous literature or the ICDD Powder Diffraction File (PDF)–4+ database. Additionally, the elemental valence states on the surface of samples were characterized with X-ray photoelectron spectroscopy (XPS; Thermo Fisher Scientific ESCALAB™ 250Xi, USA). Surface morphology and elemental distribution were characterized using field-emission scanning electron microscopy (SEM) equipped with an energy dispersive X-ray spectroscopy (EDS) instrument (JSM-IT500HR, JEOL, Japan). Quantitative elemental analysis was performed using ICP-OES (Thermo Scientific iCAP™ 7400, USA) to determine the concentration of metal ions within the solution samples. It had a measurement resolution of $10^{-3}$ μg/mL for the concentration of Li element in solution. To reduce the random error, it was standard practice to perform three replicate ICP-OES measurements on each sample solution and then use the average of these three readings as the final reported concentration for the calculation of leaching efficiency.

## Author affiliations

School of Physical Science and Technology, ShanghaiTech University, Shanghai, China.

## Statements and additional information

**Conflict of Interest** The authors declare that they have no conflict of interest.

**Acknowledgement** The authors thank Xian Meng for helping with additional ICP-OES measurements and Dr. Na Yu for helpful discussions on XRD analysis.

**Funding Information** The authors acknowledge the financial support from ShanghaiTech University. Part of the characterization experiments were conducted at the Center for High-resolution Electron Microscopy (ChEM, Grant No. EM02161943) and the Analytical Instrumentation Center (Grant No. SPST-AIC10112914) at ShanghaiTech University.

**Contributors' Statement** Jiayin Zhou: Data curation, Formal analysis, Investigation, Writing - original draft. Jingdian Liu: Data curation, Formal analysis, Investigation, Writing - original draft. Shaoyu Yang: Data curation, Formal analysis, Investigation, Writing - original draft. Chao Xu: Investigation, Resources, Writing - review & editing. Xiaofei Guan: Conceptualization, Formal analysis, Investigation, Methodology, Project administration, Resources, Supervision, Writing - review & editing.



**Supplementary Material** is available online at https://doi.org/10.1055/a-2749-6438

## References

1 Xiao J, Li J, Xu Z. Environ Sci Technol 2020; 54(01): 9–25
2 Makuza B, Tian Q, Guo X, Chattopadhyay K, Yu D. J Power Sources 2021; 491: 229622
3 Yao Y, Zhu M, Zhao Z, Tong B, Fan Y, Hua Z. ACS Sustain Chem Eng 2018; 6(11): 13611–13627
4 Wang H, Whitacre JF. Energ Technol 2018; 6(12): 2429–2437
5 Li X, Liu S, Yang J, He Z, Zheng J, Li Y. Energy Storage Mater 2023; 55: 606–630
6 Qu B, Liang J, Huo D, Li H. J Energy Storage 2025; 127: 117180
7 Larouche F, Tedjar F, Amouzegar K et al. Materials 2020; 13(03): 801
8 Cornelio A, Zanoletti A, Bontempi E. Chemistry 2024: 46
9 Zhou M, Li B, Li J, Xu Z. ACS ES&T Eng 2021; 1(10): 1369–1382
10 Chagnes A, Pospiech B. J Chem Technol Biotechnol 2013; 88(07): 1191–1199
11 Wang RC, Lin YC, Wu SH. Hydrometallurgy 2009; 99(03/04): 194–201
12 Joulié M, Laucournet R, Billy E. J Power Sources 2014; 247: 551–555
13 Lee C, Arby DS, Kim C, Lim J, Kwon K, Chung E. Hydrometallurgy 2025: 235
14 Zhao J, Zhang B, Xie H et al. Environ Res 2020; 181: 108803
15 Li L, Dunn JB, Zhang XX et al. J Power Sources 2013; 233: 180–189
16 Gao W, Liu C, Cao H et al. Waste Manag 2018; 75: 477–485
17 Lupi C, Pasquali M, Dell'Era A. Waste Manag 2005; 25(02): 215–220
18 Li Z, He LH, Zhao ZW, Wang DZ, Xu WH. ACS Sustainable Chem Eng 2019; 7(19): 16738–16746
19 Pei S, Yan S, Chen X, Li J, Xu J. Waste Manag 2024; 188: 1–10
20 Zhou J, Ni J, Guan X. RSC Sustainability 2023; 1(09): 2241–2253
21 Zhang B, Xie H, Lu B et al. ACS Sustainable Chem Eng 2019; 7(15): 13391–13399
22 Liu F, Peng C, Ma Q et al. Sep Purif Technol 2021; 259: 118181
23 Chen Y, Guan X. Processes 2025; 13(05): 1525
24 Ni J, Zhou J, Bing J, Guan X. Sep Purif Technol 2022; 278: 119485
25 Garcia-Herrero I, Margallo M, Onandía R, Aldaco R, Irabien A. Sustainable Prod Consumption 2017; 12: 44–58
26 House KZ, House CH, Schrag DP, Aziz MJ. Environ Sci Technol 2007; 41(24): 8464–8470
27 Keijer T, Bakker V, Slootweg JC. Nat Chem 2019; 11(03): 190–195
28 Binnemans K, Jones PT. J Sustainable Metall 2023; 9(01): 1–25
29 Flerlage H, Slootweg JC. Nat Rev Chem 2023; 7(09): 593–594
30 Guan X, Enalls BC, Clarke DR, Girguis P. Cryst Growth Des 2017; 17(12): 6332–6340
31 Nuraeni BA, Avarmaa K, Prentice LH, Rankin WJ, Rhamdhani MA. In Recovery of Valuable Metals from Li-Ion Battery Waste through Carbon and Hydrogen Reduction: Thermodynamic Analysis and Experimental Verification; Cham: Springer Nature Switzerland; 2023: 437–448

32 Dahlkamp JM, Quintero C, Videla A, Rojas R. Hydrometallurgy 2024; 223: 106217

33 Eshkenazi V, Peled E, Burstein L, Golodnitsky D. Solid State Ionics 2004; 170(01/02): 83–91

34 Yang Q, Zhou C, Ni J, Guan X. Sustainable Energy Fuels 2020; 4(06): 2768–2774

35 Liu Y, Wang Y, Zhao S. Curr Opin Electrochem 2023; 37: 101202

36 Meng X, Deng D. CrystEngComm 2017; 19(21): 2953–2959

37 Al-Ghoul M, El-Rassy H, Coradin T, Mokalled T. J Cryst Growth 2010; 312(06): 856–862

38 Liang R, Yonezawa S, Kim J-H, Inoue T. J Asian Ceramic Soc 2018; 6(04): 332–341

39 Wang JP. Arch Metall Mater 2021; 66(03): 745–750

40 Bhandari GS, Dhawan N. Process Saf Environ Prot 2023; 172: 523–534

41 Lee S, Park HW, Hong JP, Nam S-C, Jeon DH, Song J-H. Solid State Ionics 2022; 386: 116042